Eur. Phys. J. Plus (2023) 138:1102
https://doi.org/10.1140/epjp/s13360-023-04714-7

THE EUROPEAN PHYSICAL JOURNAL PLUS

Regular Article

Glass photonics meets photovoltaics: general principles and a case study

Francis Otieno[1,a], **Mildred Airo**[2,b], **Alex Quandt**[3,c], **Daniel Wamwangi**[3,d], **Rudolph M. Erasmus**[3,e]

[1] Department of Physics and Materials Science, Maseno University, Private Bag, Maseno, Kenya
[2] Department of Chemistry, Maseno University, Private Bag, Maseno, Kenya
[3] School of Physics, University of the Witwatersrand, Private Bag 3 Wits, Johannesburg 2050, South Africa

Received: 14 October 2023 / Accepted: 20 November 2023

Abstract In this study, we present a promising combination of glass photonics and photovoltaics to develop more efficient types of solar cells. Following up on earlier suggestions, we demonstrate that fundamental losses due to the intrinsic spectral mismatch of many photovoltaic devices can be ameliorated using spectral conversion based on rare-earth-doped glass layers. Our goal is to show work in progress in this field by approaching the topic in two ways: First, we will give a brief introduction to the basic concepts of photovoltaic devices and their intrinsic losses. Within this standard conceptual framework, we suggest that gains in efficiency due to spectral conversion layers can be described by an alternative model of absorbing and emitting solar cells, which is based on radiative transfer. Second, we practically demonstrate spectral conversion in a real device, which combines Tb-doped ZnO thin films with a typical organic solar cell. To this end, we describe in detail the fabrication of such a device using RF sputtering, carry out a typical characterization of the glass layer using Raman spectroscopy and analyze the performance of the final device.

1 Introduction

It is quite fascinating to note that an abundant raw material like sand can give rise to some of the workhorses of modern glass technologies and glass photonics [1] and also to one of the most important (quantum) semiconductor devices, which is the *p–n* junction solar cell [2]. But there is a more general problem than just a common ancestor, which brings modern glass photonics and photovoltaics together, and this is the spectral mismatch of a typical single-junction solar cells. About 50% of the incoming energy from the Sun cannot be converted into electric energy, either because the incoming photons with frequency ω cannot be absorbed when their energies $E = \hbar\omega$ are smaller than the band gap E_{gap} of the bulk absorber material. Or their energies are much larger than the band gap. Then, the free charge carriers generated by the absorbed higher energetic photons will lose a lot of their initial energies through scattering with the vibrating ionic lattice of the absorber, before they can finally be extracted at the contacts. This process is called thermalization. Both loss mechanisms are shown in Fig. 1.

Many workarounds have been suggested over the years to reduce the losses caused by spectral mismatch, which range from multi-junction solar cells to hot carrier extraction. Both approaches form the champions league of solar cell development, but are either too costly for mass production, or still plagued by fundamental problems and lack of suitable bulk materials [2]. Another idea, which was originally brought up by Trupke, Green and Würfel [3, 4], is the use of frequency conversion layers. Given a suitable combination of rare-earth ions and a suitable host material in terms of glass (ceramics), up-conversion can turn two photons with energies lower than the band gap of the bulk absorber into a photon with energy close to the band gap, and down-conversion can turn a higher energetic photon prone to thermalization losses into two photons with energies close to the band gap. That way, photons can be absorbed over a wide spectral range with minimal losses, and theoretical efficiencies between 40 and 50% have been predicted [3, 4]. These ideas will be the main topic of our study.

The paper is structured as follows: In Sect. 2, we briefly discuss the simplest theory of solar cells, which is based on the diode equation. We also present a more advanced approach, which is based on a fundamental set of equations that are used to describe a

Mildred Airo, Alex Quandt, Daniel Wamwangi, and Rudolph M. Erasmus had substantive contributions to this work.

[a] e-mail: frankotienoo@maseno.ac.ke (corresponding author)
[b] e-mail: mildredairo@gmail.com
[c] e-mail: Alex.Quandt@wits.ac.za
[d] e-mail: Daniel.Wamwangi@wits.ac.za
[e] e-mail: Rudolph.Erasmus@wits.ac.za

Published online: 12 December 2023

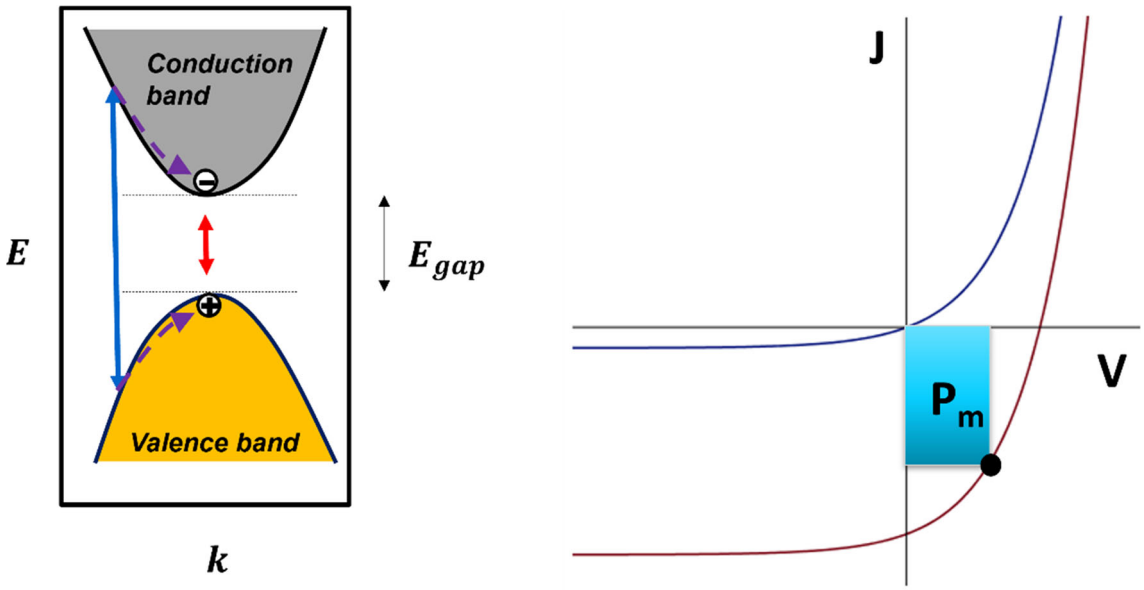

Fig. 1 (Left) Intrinsic losses in a bulk material with band gap E_{gap} due to non-absorption of red photon with energy lower than the band gap, and losses through thermalization of electrons and holes generated by a blue photon with energy much larger than the band gap. (Right) Fundamental J–V curves of a dark diode solar cell (blue) and a diode solar cell under illumination (red). The output power is characterized by the maximum working point P_m

standard photovoltaic device. Then, we discuss how spectral conversion enhances the efficiency of such devices by introducing a theory of absorbing and emitting solar cells, which is based on radiative transfer.

In Sect. 3, we give some insight into the practical use of spectral conversion in a typical solar cell device, and report from our experimental work on Tb-doped ZnO thin films as down-converting glass components in a standard organic solar cell. We describe the preparation of the ZnO thin films using RF sputtering, and we go through a detailed analysis of those films using Raman spectroscopy. A particular focus or that work is the reduction of residual stress in those layers, which is a key factor for their successful implementation as spectral conversion layers. Then, we finally explore the practical use of these films in organic solar cells either as pristine thin films, or upon doping with Tb, to serve as buffer and spectral conversion layers.

In Sect. 4, we will summarize our findings and suggest some future work.

2 Absorbing and emitting solar cells containing spectral conversion layers

In this section, we will use various theoretical approaches and concepts to describe the impact of spectral conversion on the efficiency of solar cells.

2.1 Shockley diode equation

The simplest description of the fundamental current density J vs. voltage V characteristic of a solar cell at temperature T is given by the Shockley diode equation:

$$J = J_s \cdot \left(\exp\left[\frac{eV}{nk_B T} \right] - 1 \right) - J_L \tag{1}$$

Here, J_s is a constant (the so-called saturation current density) and n an empirical quality factor between 1 and 2. The term J_L describes the light current density being generated under solar illumination. We see in Fig. 1 that the effect of the light current is to pull the typical J–V curve of a diode down in the direction of negative currents, which corresponds to power being generated by the solar cell. In other words, the bigger the photocurrent density, the more effective is the solar cell, which can be quantified by the maximum power point P_m [2]. In this simple model, an additional spectral conversion layer simply increases the light current density. The underlying mechanisms are, first of all, an extension of the energy range of available photons, and second, the reduction of thermalization losses, which would lead to a much lower light current density without spectral conversion.

2.2 The fundamental transport problem in absorbing solar cells

A more fundamental set of equations, which describes the transport of free charge carriers for purely absorbing solar cell devices in a steady state, is the following:

$$\frac{d^2\varphi(x)}{dx^2} = -\frac{e}{\varepsilon_B}\rho(x) \tag{2}$$

$$\frac{1}{e}\frac{dJ_n(x)}{dx} = -G(x) + R_n(x) \tag{3}$$

$$\frac{1}{e}\frac{dJ_p(x)}{dz} = G(x) - R_p(z) \tag{4}$$

where x is a direction perpendicular to the top area of the solar cell across the device, thus assuming a one-dimensional transport model. Equation 2 is the Poisson equation, which relates the electrostatic potential $\varphi(x)$ across the device to the density $\rho(x)$, which comprises the densities of negative (electrons) and positive (holes) free charge carriers, but also trapping and donor densities. Please note the dependence of the Poisson equation on the dielectric function ε_B of the absorbing bulk material. Equations 3 and 4 are continuity equations, which relate the current densities J_n for electrons and J_p for holes to the photogeneration rate $G(x)$, and these equations also contain specific recombination rates $R_n(x)$ and $R_p(x)$. Thus, the absorption of incoming photons and the subsequent generation of free charge carriers lead to a photogenerated source term $G(x)$ in both continuity equations, whereas the recombination processes of free charge carriers lead to sink terms $R_n(x)$ and $R_p(x)$. The fundamental set of Eqs. (2–4), together with the specification of boundary conditions to model the contacts, are the basis of state-of-the-art solar cell device simulations [5]. Ignoring reflectivity at the surface, the photogeneration rate $G(x)$ in this model depends on the absorption coefficient $\alpha(E)$ of the absorbing bulk material and on the photon flux $b(E, x)$. For details, see [2] or [7]. Spectral conversion processes will clearly modify the photon flux $b(E, x)$, and as a result, we expect to see increases in the photogeneration rate, which leads to larger current densities of free charge carriers and finally to increases in the resulting device efficiency.

2.3 Charge carrier transport in absorbing and emitting solar cells

Based on the set of equations described in the previous section, one can apply an ad hoc approach to describe the effect of spectral conversion layers on the incoming photon flux $b(E, x)$. This approach is based on the rate equations that describe a system of rare-earth ions being pumped by solar radiation rather than by a laser source. We have explored this approach in the framework of solar cell device simulations [6, 7], and the results were acceptable, but the approach itself was not very elegant.

In the following, we will suggest a more general approach to introduce spectral conversion into the transport problem of solar cells. This approach is based on the equations of radiative transfer. The idea itself is very simple. We note that the (specific) intensity $I(E, x)$ of the incoming radiation in an absorbing and emitting solar cell may be described by the following equation of radiative transfer [8]:

$$\frac{\mathrm{d}I(E,x)}{\mathrm{d}x} = -\alpha(E)I(E,x) + j(E) \tag{5}$$

Note that $\alpha(E)$ is the absorption coefficient and $j(E)$ the emission coefficient of the bulk material. This equation is readily solved (i.e., by using Laplace transforms) and we obtain:

$$I(E,x) = I(E,0)e^{-\alpha(E)\cdot x} + \frac{j(E)}{\alpha(E)}\left(1 - e^{-\alpha(E)\cdot x}\right) \tag{6}$$

The first term in this solution describes the exponential decay of the intensity, which is known as Beer's law [2]. The second term describes a growing intensity due to emission. Note that the intensity $I(E, x)$ is directly related to the photon flux $b(E, x)$ within the solar cell by $b(E, x) = \frac{I(E,x)}{E}$, which gives the modified photon flux for an absorbing and emitting solar cell. Finally, this modified photon flux must be used in the expression for the photogeneration rate $G(x)$.

The suggested approach based on radiative transfer becomes most powerful, if one is able to establish approximate relations between the absorption coefficients and the emission coefficients in the case of spectral conversion processes. The absorption coefficients are usually much easier to determine than the emission coefficients, and in particular when using first principles methods [9]. For the ideal case of a black body at temperature T, the relation between its absorption coefficient and its emission coefficient amounts to $\frac{j(E)}{\alpha(E)} = B(E, T)$, where $B(E, T)$ is the spectral radiance of that black body [10]. Furthermore, McCumber [11] has derived a relation between absorption and emission cross sections, which refers to what could be characterized as a dirty two-level system and which might also be an interesting starting point in this regard. Further details are work in progress, and they will be discussed elsewhere.

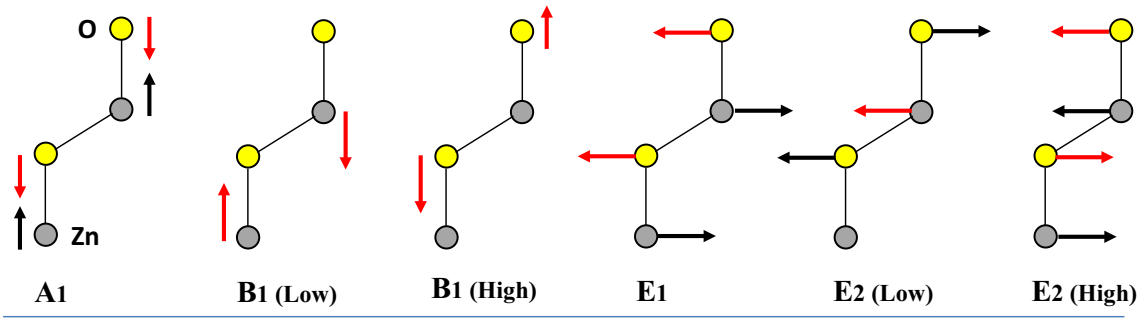

Fig. 2 Eigenvectors of the ZnO optical phonon modes. For every mode, the red arrows represent the dominating displacement vectors. The A_1, B_1 (high), E_1 and E (high) modes are oxygen-dominated, while B (low) and E_2 (low) modes are Zn-displacement dominated

3 A case study: organic solar cells with ZnO-based spectral conversion layers

Interest in the development of bulk heterojunction organic solar cells has continuously increased over the years, because of their low cost and because of improvements in device efficiencies, which have recently surpassed the 19% threshold [12–14]. At this rate, the photoconversion efficiency (PCE) in organic photovoltaics (OPV) will soon surpass the efficiency of the more costly Si based PV. This enhancement is driven primarily by the development of novel polymers such as non-fullerene acceptors, which have shown excellent optical properties, a modulation of the photoactive layer to form ternary heterojunctions with an extended absorption range, and lastly the incorporation of spectrum conversion layers. While the first two strategies have already led to larger improvements in the performance of OPV devices, light management through plasmonic and frequency conversion offers further advantages in the extension of PCE values, which would be comparable to those of multi-junction devices [15, 16]. In this section, we present as a proof of concept the efficiency enhancement strategy of an organic solar cell based on non-fullerene acceptor polymer, where we use rare-earth-doped ZnO as the glass photonic spectral conversion layer. The dual effect of applying a non-fullerene acceptor (NFA) derivative and rare-earth-doped trivalent elements in ZnO in a typical inverted organic solar cell device nicely illustrates the practical use of combining glass photonics and photovoltaics [17]. In the subsequent sections, we will study the physical properties of these thin-film ZnO layers, which were fabricated by RF sputtering and subsequent thermal annealing to improve their structural and optoelectronic properties.

3.1 Properties of ZnO thin films

ZnO is a transparent conducting wide band gap semiconductor with extensive applications in optoelectronic devices [18, 19]. From the point of view of glass photonics, it provides a direct band gap and strong absorption in the near-UV spectral region. Therefore, it is also used as a template photoelectrode and as an electron transport layer for various solar cell applications. Additionally, the large energy band gap may be modified through doping with rare-earth elements to allow for tunable frequency conversion. These properties make ZnO a rather unique glass photonic component for practical implementations of spectral conversion layers. The efficiency of these layers is highly dependent on the crystal structure and even nano structural characteristics of the host material, where size effects and fundamental interactions may strongly affect the basic energy transfer mechanisms. Here, Raman spectroscopy may be used to analyze the electron–hole pair interaction with the phonons propagating in the wurzite–ZnO through an inelastic scattering process [20, 21]. Then, the phase purity of the wurtzite lattice of ZnO is probed by the analysis of the 12 vibrational eigenmodes corresponding to the P63mc space group. As such, we identify the essential three acoustic $\Gamma = 2A_1 + 2B_1 + 2E_1 + 2E_2$ and nine optical phonons, $\Gamma_{\text{optical}} = A_1 + 2B_1 + E_1 + 2E_2$. That determine atomic configurations in the respective unit cells and the corresponding phonon modes over the Brillouin zone [22]. These vibrational modes characterize the structural and composition purity of ZnO compound in the bulk and in the thin films.

The dominant optical and acoustic modes also include E_1(TO), E_1(LO), E_2 (high), which can be signatures of defects and vacancies in ZnO. These modes are illustrated by their respect atomic displacements in Figs. 2 and 3 for bulk ZnO with six first-order Raman active modes. More details on the polar and non-polar Raman active modes in ZnO can be found in [23], [24].

3.2 Experimental

3.2.1 Growth of ZnO thin films for PV applications

The properties and the quality of the glass photonic layers are highly dependent on the fabrication methods. For the present study, ZnO and Tb-doped ZnO thin films have been deposited by RF magnetron sputtering of a ZnO target of purity 99.95% on (100) Si and quartz substrates. The substrates were thoroughly cleaned with organic solvents and dried prior to film deposition with a vacuum chamber of base pressure 1.8×10^{-5} mbar. Plasma ignition was carried out in an argon gas atmosphere at a flow rate of 13.0 sccm.

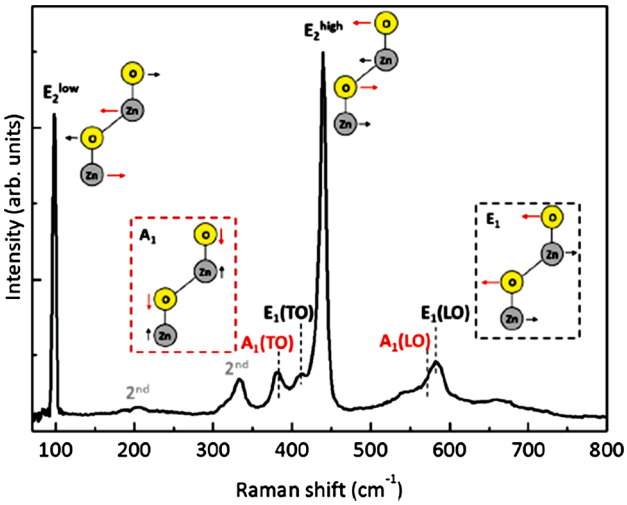

Fig. 3 Unpolarized Raman spectrum of bulk ZnO showing Raman active modes with the corresponding vibrations of the ions. The red arrows specify the dominant ionic displacements

The RF power and the deposition time for the ZnO were varied from 100 to 260 W and between 1 and 20 min for variation of the physical properties of the ZnO thin film as verified by Raman spectroscopy. The Tb-doped ZnO thin films were deposited at room temperature, and in the organic solar cells, they served as electron transport and spectral conversion layers. We finally compared the performance of these devices to the performance of reference OPV devices with pristine ZnO layers, in order to probe the effect of spectral conversion.

3.2.2 OPVs device fabrication

In this subsection, we describe the procedures for fabricating an inverted organic solar cell device containing ZnO and Tb-doped ZnO as an electron transport layers and/or frequency conversion layers. Pristine ZnO layers of thickness 120 nm were foremost deposited onto an ITO-coated glass substrate at 100 W for 1 min. Subsequently, the photoactive layer of a PTB7:ITIC-4F polymer blend solution (Sigma-Aldrich) in dichlorobenzene was prepared at 1:1 mass ratio and with a total concentration of 20 mg/ml. This mixed solution was spin-coated at 2000 rpm for 60 s to form a homogenous film of 215 nm thickness serving as the electron transport layer. Thereafter, PEDOT:PSS (1.3 wt% dispersion in H_2O) was spin-coated at the same speed to form a hole transport layer. The final step was a metallization of the device with aluminum, which was deposited through thermal evaporation at high vacuum. These procedures lead to a device with inverted architecture in the form ITO/photonic layer/PTB7:ITIC-4F/PEDOT:PSS/Al. The resulting device was finally annealed in Argon ambient at 100 ˚C for 15 min to remove organic polymer solvent and any residual water.

3.3 Results and discussion

The optimum ZnO thin film was found by a series of characterizations that would probe elemental composition, high phase purity and microstructural quality. All properties strongly influence the optoelectronic behavior of ZnO layers through quantum confinement effects, and they are crucial for their dual function as an electron transport and as a frequency conversion layer. The following sections summarize the results of these characterizations.

3.3.1 Elemental composition

The elemental composition of the ZnO thin films was determined using Energy Dispersive X-ray Spectrometry (EDS). Thin films containing Tb (reported earlier in [25] using Rutherford backscattering spectroscopy) were marked by the absence of impurities during their growth, which is also evident from the EDS spectrum of Fig. 4.

A similar analysis of our Tb–ZnO thin film using EDS essentially confirmed the composition and the microstructural purity of these layers.

3.3.2 Raman spectroscopy analysis

Band alignment in organic solar cells is a critical parameter that determines the efficiency of charge transport and recombination channels [26, 27], and it strongly guides the choice of the photonic layers to be incorporated as the electron transport layer. The characteristics of a typical electron transport layer reveal its dual role: first, in reducing the lifetime of the charge carriers through optimal energy band offset, which can be tuned by microstructure modification to induce quantum size confinement effects on/within the host compound. Additionally, this layer should selectively block the unwanted charge carriers through mobility filtering [28].

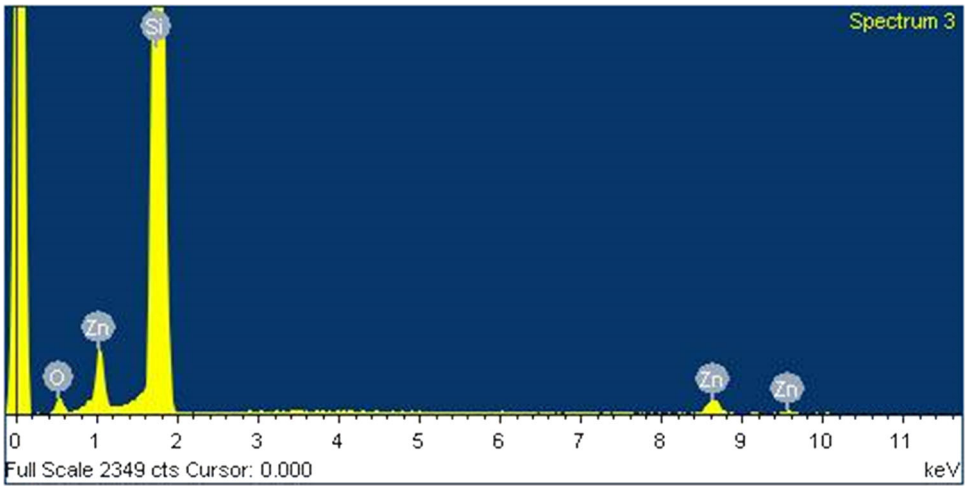

Fig. 4 EDS analysis of the ZnO thin film grown using RF sputtering on a Si wafer substrate

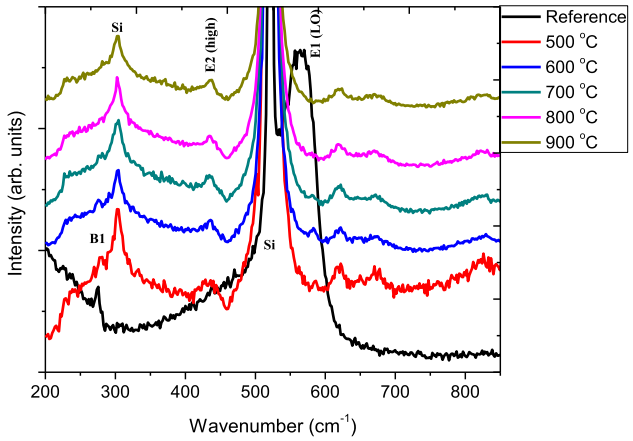

Fig. 5 Raman spectra of ZnO thin film grown at 100 W for 1 min, before and after annealing the film at temperatures between 500 and 900 °C

Concerning the photonic layers, the tuning of their microstructures would involve energetic parameters (RF power) and kinetic parameters (deposition time), and their functionality was further enhanced by incorporating rare-earth ions [29]. Moreover, the formation of multilayers using thin-film deposition techniques always requires a balance between their residual stresses, which is discussed in the following sections.

Effect of annealing on ZnO thin films deposited for 1 min Figure 5 shows the Raman spectra of a ZnO thin film deposited on Si (001) for 1 min at an RF power of 100 W. The film had a thickness of 120 nm and was annealed for 2 h under an argon atmosphere in a temperature range of 500–900 °C. The strong peak of the reference film round 434.5 cm^{-1} is assigned to the non-polar optical phonons E_2 (high) modes of the ZnO film. The peaks at 522 and 303 cm^{-1} are attributed to the optical phonon modes of the silicon substrate, and the broad peak at about 565 cm^{-1} is attributed to the E_1 (LO) mode of ZnO. After annealing, the E_2 phonon frequency is blue shifted from 434.5 to 437 cm^{-1}. This shift of 2.5 cm^{-1} is a strong indication for a decrease in the tensile stresses within the layer.

Effect of annealing film grown using 5-min deposition To further determine the effects of film thickness and annealing on the tensile stress in ZnO thin films, we also used deposition times of 5 min. The resulting film thickness was measured to be 132 nm. The results of the structural properties after annealing are shown in Fig. 6. It is evident that the E_2 (high) mode is very sensitive to deposition time, since it appears at a lower wavenumber of 432 cm^{-1} compared to that of a film grown for 1 min. The decrease of the wavenumber with increasing deposition time is indicative of increasing tensile stresses with these thin films.

Effect of annealing film grown using 20-min deposition An increasing tensile stress is also evident for films grown with 20-min deposition time (Fig. 7). Those films had a thickness of 230 nm. The tensile stresses are attributed to the atomic peening effect, which locally increases the temperature gradient between the film and the substrate, and it leads to a pronounced mismatch in thermal stresses.

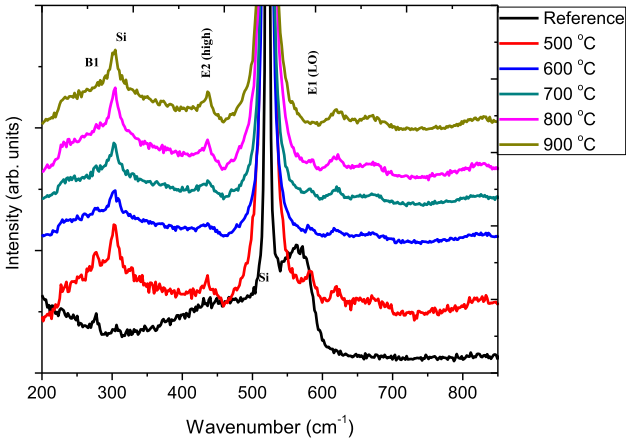

Fig. 6 Raman spectra of ZnO thin film grown at 100 W for 5 min, before and after annealing the film at temperatures between 500 and 900 °C

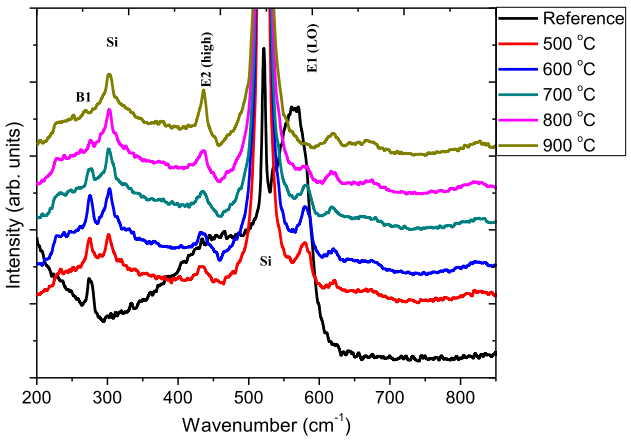

Fig. 7 Raman spectra of ZnO thin film grown at 100 W for 20 min, before and after annealing the film at temperatures between 500 and 900 °C

Effect of varying thin-film deposition time To determine the effect of microstructure on the film properties, we carried out a systematic annealing study of films grown to a different thickness. A general comparison of the Raman spectra of ZnO thin films as a function of deposition time is shown in Fig. 8. Our results demonstrate the appearance of the B_1 silent inactive mode in the vicinity of 275 cm^{-1}. This mode is gradually red shifted shift to 277 cm^{-1} for films grown over 20 min. The presence of this mode conforms to earlier work by Serrano et al. [30], whose theoretical calculations attribute this mode to the displacement vectors of Zn- and O-sublattices during the presence of symmetry breaking defects, grain boundary impurities or localized electric field distributions [30–33]. The disappearance of this mode with annealing temperature indicates enhanced crystallinity, which would generally require higher annealing temperatures for thicker films. This observation emphasizes again the necessity to establish optimal growth conditions in order to obtain enhanced thin-film properties.

The controversial but silent E_1 (LO) phonon mode at 580 cm^{-1} confirms the wurtzite hexagonal phase in the ZnO films fabricated by RF sputtering [34, 35] and [36]. The presence of this peak may indicate the existence of native defects that are correlated to thermally activated particle size effects. The latter drive a competition between the surface and volume effects to minimize the number of defect states, which is strongly suggested by decreasing scattering intensities of the respective phonon modes [37]. We also observe the disappearance of this peak at 700 °C, 800 °C and 900 °C for the 1-min, 5-min and 20-min deposition times, respectively. It is well known that thermal activation leads to the decrease in oxygen vacancies, and therefore, the reduction in peak intensity could be attributed to the recombination with oxygen interstitials or migration into sinks [36]. According to Al Asmar et al. [38] the 580 cm^{-1} peak refers to charge trapping at grain boundaries and the presence of localized interface and/or surface phonon modes. On annealing, the grain boundary density is gradually reduced as the grain size increases. In consequence, the charge trapping effect at grain boundaries vanishes when the annealing temperature increases. And finally, we observe that the E_2 (high) peak gradually increases in intensity, similar to the film grown for 5-min deposition time. In both cases, the pristine films are partially crystalline due to the low signal-to-noise ratio of the E_2 mode of the reference films.

Effect of varying thin-film deposition RF power The Raman spectra as a function of RF sputtering power are shown in Fig. 9. One notices the distinct Raman peaks at 275 cm^{-1}, 522 cm^{-1} and 565 cm^{-1}. The sharp 522 cm^{-1} peak corresponds to Si phonon modes. The 275 cm^{-1} peak is attributed to the B_1 silent inactive mode. It slightly shifts to 277 cm^{-1}, and we observe an increasing peak intensity with increasing deposition time. This shift in the peak position could be attributed to a decrease in tensile strain.

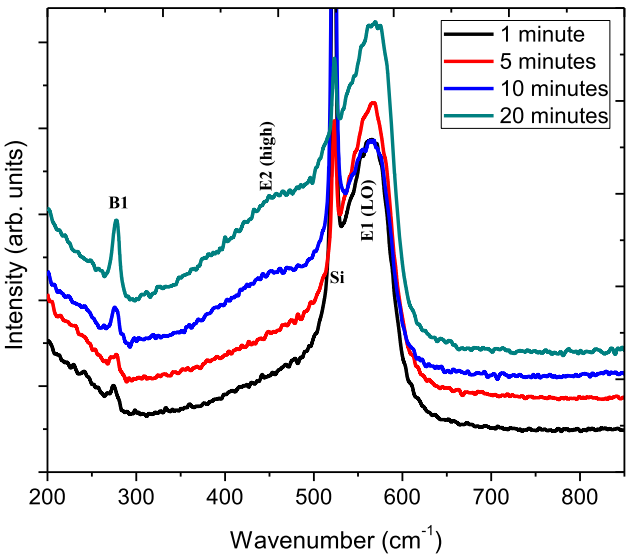

Fig. 8 Raman spectra of ZnO thin film grown at 100 W for different deposition times (1–20 min)

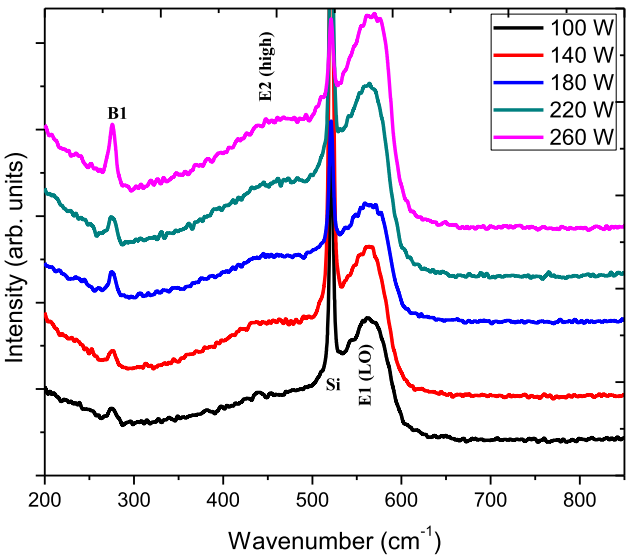

Fig. 9 Raman spectra of ZnO thin film grown for 5 min at different RF powers (100–260 W)

According to Manova et al. [39], the use of controlled energetic ion bombardment in thin-film formation leads to improved adhesion, reduced substrate temperatures, the control of intrinsic stress and adjustments of surface texture, phase formation and nano-topography. Our results agree with these observations, and we see an evident shift in the peak positions with increasing RF power, which reflects the phase transition from amorphous to highly crystalline growth. The films deposited at 260 W power showed a sharp crystalline B_1 silent inactive mode peak at 277 cm^{-1}, which indicates that the crystallization of our thin films increases with increasing RF power.

In summary, all of our structural characterizations confirm that thermal activation minimizes the number of native defects effects and also reduces tensile stress. These features are essentially good news for OPV device application, and particularly in the inverted device architecture. In the next section, we finally study the use of ZnO layers in a typical photovoltaic application.

3.4 Applications of pristine and Tb-doped ZnO thin films in organic solar cells

This section describes the measured performance of ZnO-based thin films as electron transport layers and as frequency conversion layer in a typical inverted organic solar cell. Figure 10 shows the current density to voltage (J–V) characteristics under AM 1.5 irradiation conditions for two prototype OPV devices with pristine ZnO and Tb-doped ZnO layers. The inverted structure of these prototype devices was ITO/ZnO:Tb^{3+}/PTB7:ITIC-4F/PEDOT:PSS/Al, where the ZnO and ZnO:Tb^{3+} thin films were obtained using RF sputtering onto ITO-coated glass substrates. The films used for device fabrication have not been subjected to annealing due to the floppy behavior of ITO glass substrates, which soften at T >400 °C. Furthermore, annealing may lead to the thermally activated diffusion of indium, which deteriorates the electrical properties of the ITO films.

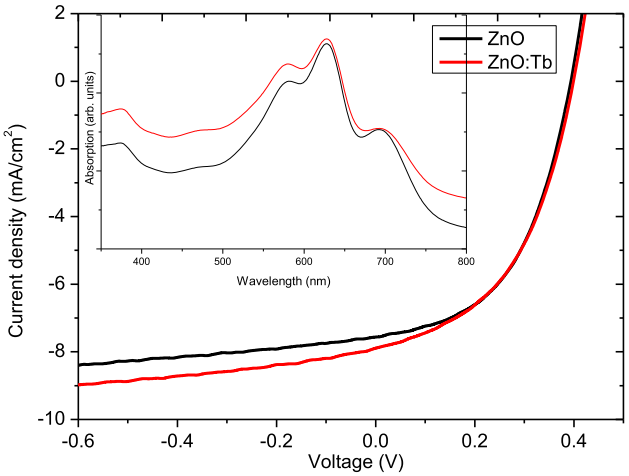

Fig. 10 J–V characteristics of devices formed using pristine and Tb-doped ZnO as the layers. The inset shows the UV–visible absorption spectra of the active layer with different ZnO layers

The open circuit voltage, series resistances and the fill factor of the two devices remained unaltered, which indicates that the electronic properties of ZnO layers have not been altered by Tb doping. The short circuit current density increases from 7.5 to 7.9 mA/cm^2, which indicates the spectral down-conversion due to the presence of Tb atoms in the ZnO layer. The enhanced photocurrent corroborates with the absorption measurements shown in the inset. There is an obvious increase in the absorption range after introducing the Tb atoms, which leads to an enhanced number of photons in the visible region after converting higher energetic photons in the UV region. The spectral conversion process has modified the UV properties of the original solar emission spectrum, and it leads to an enhanced photo-absorption in the π–π^* transition of the donor polymer in solar cell and thus to a larger concentration of free charge carriers. This is a very promising result, and a nice practical example for the significance of glass photonics to improve the efficiencies of photovoltaic devices.

4 Conclusion

With this study, we want to point out the use of glass photonics as a very promising strategy to increase the efficiency of standard photovoltaic devices. The suggested techniques can be modified to allow for a variety of rare-earth-doped glass (ceramics) layers to be deposited on standard photovoltaic devices. And with the necessary meticulous fine tuning and cleaner fabrication methods, spectral conversion based on glass photonics may be taken from the conceptual stage with relatively low gains in efficiency closer to the theoretical gains described in the literature.

From a theoretical and conceptual point of view, we discussed the main aspects of the standard approaches to describe photovoltaic devices, and we pointed out intrinsic and rather fundamental losses due to spectral mismatch in this framework. Then, we picked up earlier suggestions in the literature, where authors have strongly advertised the use of spectral conversion based on rare-earth-doped glass layers to circumvent spectral losses, and to increase the efficiency of standard photovoltaic devices. Based on their ideas, we developed a more general theoretical and conceptual framework of absorbing and emitting solar cells, which was derived from the basic equations of radiative transfer. We are optimistic that by systematically expanding on older approaches based on non-ideal black body emitters, this general framework may be taken from the conceptual stage toward its final implementation in standard solar cell device simulations.

From a practical point of view, we also demonstrated the practical implementation of spectral conversion in solar cells based on glass photonics. To this end, we described in detail how ZnO thin films with different thicknesses and different annealing temperatures were prepared on silicon substrates by RF magnetron sputtering. The pressure in the vacuum chamber during the deposition was lower than 5×10^{-5} Pa. Using Raman spectroscopy studies, the surface structure was studied as a function of deposition rate and post-deposition annealing temperature, with a temperature range of 500–900 °C. The films show a peak near 275 cm^{-1} attributed to the B_1 silent inactive mode which drastically reduces intensity with annealing temperature, and we pointed out further dependencies on deposition time and power. The incorporation of pristine and Tb-doped ZnO thin films into organic solar cell device resulted in an increase in absorption below and beyond the visible range, which is an indication that these films can be used as a buffer layer and as a down-conversion layer to enhance the OPV device performance.

Acknowledgements The authors would like to thank the ARUA Early-Career Research Fellowship 2022 that enabled completion of the manuscript preparations, the ARUA Centre of Excellence in Materials, Energy and Nanotechnology (CoEMEN) hosted at the School of Physics, University of the Witwatersrand, for being host during the fellowship and Department of Physics and Materials Science, School of Physical and Biological Sciences, Maseno University.

Data Availability Statement Datasets generated during the current study are available from the corresponding author on reasonable request. This manuscript has associated data in a data repository. [Authors' comment: Data sets generated during the current study are available from the corresponding author on reasonable request.]

References

1. J.E. Shelby, Introduction to glass science and technology. 2020: royal society of chemistry (2020)
2. J.A. Nelson, The physics of solar cells. 2003: World scientific publishing company (2003)
3. T. Trupke, M. Green, P. Würfel, Improving solar cell efficiencies by down-conversion of high-energy photons. J. Appl. Phys. **92**(3), 1668–1674 (2002)
4. T. Trupke, M. Green, P. Würfel, Improving solar cell efficiencies by up-conversion of sub-band-gap light. J. Appl. Phys. **92**(7), 4117–4122 (2002)
5. P. Sharma et al., Si and GaAs SIS heterostructure solar cells using spray-deposited ITO. Jpn. J. Appl. Phys. **19**(S1), 551 (1980)
6. A. Quandt et al., About the implementation of frequency conversion processes in solar cell device simulations. Micromachines **9**(9), 435 (2018)
7. A. Quandt, I. Mokgosi, R. Warmbier, Simulations of conventional and augmented types of solar cells, in *Solar Cells and Light Management*. (Elsevier, 2020), pp.249–276
8. S. Chandrasekhar, Radiative transfer: Courier Corporation. (2013)
9. A. Quandt, R. Warmbier, Solar cell simulations based on ab initio methods. Opt. Mater. Expr. **11**(6), 1763–1779 (2021)
10. M. Weinstein, On the validity of Kirchhoff's law for a freely radiating body. Am. J. Phys. **28**(2), 123–125 (1960)
11. D. McCumber, Einstein relations connecting broadband emission and absorption spectra. Phys. Rev. **136**(4A), A954 (1964)
12. Y. Cui et al., Single-junction organic photovoltaic cell with 19% efficiency. Adv. Mater. **33**(41), 2102420 (2021)
13. C. Han et al., Over 19% efficiency organic solar cells by regulating multidimensional intermolecular interactions. Adv. Mater. **35**(10), 2208986 (2023)
14. H. Chen et al., A 19% efficient and stable organic photovoltaic device enabled by a guest nonfullerene acceptor with fibril-like morphology. Energy Environ. Sci. **16**(3), 1062–1070 (2023)
15. P. Gibart et al., Below band-gap IR response of substrate-free GaAs solar cells using two-photon up-conversion. Jpn. J. Appl. Phys. **35**(8R), 4401 (1996)
16. T. Ameri et al., Organic ternary solar cells: a review. Adv. Mater. **25**(31), 4245–4266 (2013)
17. Z. Li et al., High-efficiency, mass-producible, and colored solar photovoltaics enabled by self-assembled photonic glass. ACS Nano **16**(7), 11473–11482 (2022)
18. V. Karpina et al., Zinc oxide–analogue of GaN with new perspective possibilities. Cryst. Res. Technol. J. Exp. Ind. Crystall. **39**(11), 980–992 (2004)
19. Ü. Özgür et al., A comprehensive review of ZnO materials and devices. J. Appl. Phys. **98**(4), 11 (2005)
20. Y. Peter, M. Cardona, Fundamentals of semiconductors: physics and materials properties. 2010: Springer Science & Business Media. (2010)
21. J.-H. Fan et al., Resonance Raman scattering in bulk 2H-MX_2 (M= Mo, W; X= S, Se) and monolayer MoS_2. J. Appl. Phys. **115**(5), 053527 (2014)
22. R. Loudon, The Raman effect in crystals. Adv. Phys. **13**(52), 423–482 (1964)
23. A. Iqbal, M. Zakria, A. Mahmood, Structural and spectroscopic analysis of wurtzite $(ZnO)_{1-x}(Sb_2\ O_3)_x$ composite semiconductor. Progr. Nat. Sci. Mater. Int. **25**(2), 131–136 (2015)
24. C. Klingshirn, ZnO: from basics towards applications. Phys. Status Solidi (b) **244**(9), 3027–3073 (2007)
25. F. Otieno et al., Effect of thermal treatment on ZnO: Tb^{3+} nano-crystalline thin films and application for spectral conversion in inverted organic solar cells. RSC Adv. **8**(51), 29274–29282 (2018)
26. S. Izawa, N. Shintaku, M. Hiramoto, Effect of band bending and energy level alignment at the donor/acceptor interface on open-circuit voltage in organic solar cells. J. Phys. Chem. Lett. **9**(11), 2914–2918 (2018)
27. H. Luo et al., Understanding the effects of the energy band alignment at the donor/acceptor interface on the open circuit voltage of organic photovoltaic devices. Chem. Phys. Lett. **711**, 113–117 (2018)
28. B. Ebenhoch et al., Charge carrier mobility of the organic photovoltaic materials PTB7 and PC71BM and its influence on device performance. Org. Electron. **22**, 62–68 (2015)
29. N. Wu et al., The preparation of a Eu^{3+}-doped ZnO bi-functional layer and its application in organic photovoltaics. Mater. Res. Expr. **2**(12), 125901 (2015)
30. J. Serrano et al., Pressure dependence of the lattice dynamics of ZnO: an ab initio approach. Phys. Rev. B **69**(9), 094306 (2004)
31. M. Tzolov et al., Modification of the structure of ZnO: Al films by control of the plasma parameters. Thin Solid Films **396**(1), 276–281 (2001)
32. J. Dong et al., Effects of hydrogen plasma treatment on the electrical and optical properties of ZnO films: identification of hydrogen donors in ZnO. ACS Appl. Mater. Interfaces **2**(6), 1780–1784 (2010)
33. V. Russo et al., Multi-wavelength Raman scattering of nanostructured Al-doped zinc oxide. J. Appl. Phys. **115**(7), 073508 (2014)
34. F. Manjón et al., Silent Raman modes in zinc oxide and related nitrides. J. Appl. Phys. **97**(5), 053516 (2005)
35. A. Kaschner et al., Nitrogen-related local vibrational modes in ZnO: N. Appl. Phys. Lett. **80**(11), 1909–1911 (2002)
36. Z. Chen et al., Microvoid formation in hydrogen-implanted ZnO probed by a slow positron beam. Phys. Rev. B **71**(11), 115213 (2005)
37. K. Saravanakumar et al., XPS and Raman studies on (002) oriented nanocrystalline ZnO films showing temperature dependent optical red shift. Adv. Stud. Theor. Phys. **5**(4), 155–170 (2011)
38. R. Al Asmar et al., Characterization and Raman investigations on high-quality ZnO thin films fabricated by reactive electron beam evaporation technique. J. Cryst. Growth **279**(3–4), 394–402 (2005)
39. D. Manova, J.W. Gerlach, S. Mändl, Thin film deposition using energetic ions. Materials **3**(8), 4109–4141 (2010)